A. Caporale et alii, Frattura ed Integrità Strutturale, 29 (2014) 19-27; DOI: 10.3221/IGF-ESIS.29.03

Focussed on: Computational Mechanics and Mechanics of Materials in Italy

A micromechanical four-phase model to predict the compressive failure surface of cement concrete

A. Caporale, R. Luciano
Department of Civil and Mechanical Engineering, University of Cassino and Southern Lazio
a.caporale@unicas.it, luciano@unicas.it

ABSTRACT. In this work, a micromechanical model is used in order to predict the failure surface of cement concrete subject to multi-axial compression. In the adopted model, the concrete material is schematised as a composite with the following constituents: coarse aggregate (gravel), fine aggregate (sand) and cement paste. The cement paste contains some voids which grow during the loading process. In fact, the non-linear behavior of the concrete is attributed to the creation of cracks in the cement paste; the effect of the cracks is taken into account by introducing equivalent voids (inclusions with zero stiffness) in the cement paste. The three types of inclusions (namely gravel, sand and voids) have different scales, so that the overall behavior of the concrete is obtained by the composition of three different homogenizations; in the sense that the concrete is regarded as the homogenized material of the two-phase composite constituted of the gravel and the mortar; in turn, the mortar is the homogenized material of the two-phase composite constituted of the sand inclusions and a (porous) cement paste matrix; finally, the (porous) cement paste is the homogenized material of the two-phase composite constituted of voids and the pure paste. The pure paste represents the cement paste before the loading process, so that it does not contain voids or other defects due to the loading process. The above-mentioned three homogenizations are realized with the predictive scheme of Mori-Tanaka in conjunction with the Eshelby method. The adopted model can be considered an attempt to find micromechanical tools able to capture peculiar aspects of the cement concrete in load cases of uni-axial and multi-axial compression. Attributing the non-linear behavior of concrete to the creation of equivalent voids in the cement paste provides correspondence with many phenomenological aspects of concrete behavior. Trying to improve this correspondence, the influence of the parameters of the evolution law of the equivalent voids in the cement paste is investigated, showing how the parameters affect the uni-axial stress-strain curve and the failure surfaces in bi-axial and tri-axial compression.

KEYWORDS. Cement concrete; Micromechanics; Compressive strength.

INTRODUCTION

Micromechanical methods [1-3] have been widely used to homogenize fiber reinforced composites such as FRP, frequently employed to strengthen existing structures made of concrete [4-8]. Micromechanics has also been adopted for the analysis of different types of heterogeneous materials such as masonry arrangements [9,10] and cement concrete [11-16]. In [17], a four-phase micromechanical model has been proposed in order to simulate the non-linear instantaneous pre-peak response of cement concrete subjected to monotonically increasing loads of uni-axial

compression. In this work, the micromechanical model presented in [17] is used in order to predict the failure surface of cement concrete subject to multi-axial compression. It is underlined that stress-strain curves in uni-axial compression are provided in [17], whereas failure curves in the plane of the principal stresses in concrete are considered in this work. The failure curves provided by the proposed micromechanical method can also be obtained with experimental tests which involve high economical costs as equipment able to impose bi-axial and tri-axial states of compression is required. The aim of the work is to determine theoretically the mechanical parameters that affect more the behavior of cement concrete in order to reduce the number of expensive experimental tests on concrete specimens.

MICROMECHANICAL MODEL

In the proposed model, the concrete material is viewed as a composite with the following constituents: coarse aggregate (gravel), fine aggregate (sand) and cement paste. The cement paste contains some voids which grow during the loading process. In fact, the non-linear behavior of the concrete is attributed to the creation of cracks in the cement paste; the effect of the cracks is taken into account by introducing equivalent voids (inclusions with zero stiffness) in the cement paste. The three types of inclusions (namely gravel, sand and voids) have different scales, so that the overall behavior of the concrete is obtained by the composition of three different homogenizations; in the sense that the concrete is regarded as the homogenized material of the two-phase composite constituted of the gravel and the mortar; in turn, the mortar is the homogenized material of the two-phase composite constituted of the sand inclusions and a (porous) cement paste matrix; finally, the (porous) cement paste is the homogenized material of the two-phase composite constituted of voids and the pure paste; the pure paste represents the cement paste before the loading process, so that it does not contain voids or other defects due to the loading process. The pure paste can contain defects but these are due to the production process of the cement paste and not to the loading process. The above-mentioned three homogenizations are realized with the predictive scheme of Mori-Tanaka in conjunction with the Eshelby method, frequently used in the homogenization of composites [11,13].
The micromechanical method described in [17] provides the stress in the concrete material subject to a prescribed strain and, vice versa, the strain in concrete material subject to a prescribed stress. The volume fraction of the voids in the cement paste is denoted by f_v. The overall elasticity of the porous cement paste, mortar and concrete are denoted by $\bar{\mathbf{C}}^{(p)}$, $\bar{\mathbf{C}}^{(m)}$ and $\bar{\mathbf{C}}^{(c)}$, respectively. Considering that the paste is composed of pure paste and voids, the overall elasticity $\bar{\mathbf{C}}^{(p)}$ of the paste is a function of the volume fraction f_v of the voids. As a consequence, the overall elasticity of mortar and concrete are also functions of f_v. The overall elasticity of paste, mortar and concrete are evaluated with the Mori-Tanaka method in conjunction with the result of the Eshelby's problem of an ellipsoidal inclusion in a homogeneous, linearly elastic and infinitely extended medium (see also [17]). The overall compliances of the cement paste, mortar and concrete are denoted by $\bar{\mathbf{D}}^{(p)}$, $\bar{\mathbf{D}}^{(m)}$ and $\bar{\mathbf{D}}^{(c)}$, respectively; these compliances are obtained by inverting the corresponding overall elasticity and are also functions of f_v:

$$\begin{aligned}
\bar{\mathbf{D}}^{(p)}\left(f_v\right) &= \left(\bar{\mathbf{C}}^{(p)}\left(f_v\right)\right)^{-1} \\
\bar{\mathbf{D}}^{(m)}\left(f_v\right) &= \left(\bar{\mathbf{C}}^{(m)}\left(f_v\right)\right)^{-1} \\
\bar{\mathbf{D}}^{(c)}\left(f_v\right) &= \left(\bar{\mathbf{C}}^{(c)}\left(f_v\right)\right)^{-1}
\end{aligned} \tag{1}$$

In this work, a macro-stress $\boldsymbol{\sigma}^{\infty}$ is prescribed to the concrete and the average stress and strain in the constituents of concrete and corresponding to $\boldsymbol{\sigma}^{\infty}$ are evaluated with the following iterative procedure, which makes use of a secant approach. The value of the void volume fraction f_v at the generic ith iteration is denoted by $f_{v,i}$. The average stress and strain in the constituents of concrete at the generic ith iteration are evaluated by assuming that it is known $f_{v,i-1}$, i.e. the void volume fraction at the previous iteration $i-1$. Specifically, the following overall elasticity and compliance corresponding to $f_{v,i-1}$ are evaluated in the ith iteration of the procedure:

$$\bar{\mathbf{C}}^{(p)}\left(f_{v,i-1}\right), \bar{\mathbf{C}}^{(m)}\left(f_{v,i-1}\right), \bar{\mathbf{C}}^{(c)}\left(f_{v,i-1}\right), \bar{\mathbf{D}}^{(p)}\left(f_{v,i-1}\right), \bar{\mathbf{D}}^{(m)}\left(f_{v,i-1}\right), \bar{\mathbf{D}}^{(c)}\left(f_{v,i-1}\right) \tag{2}$$

It is noted that the iterative procedure begins with the first iteration ($i=1$), where the void volume fraction $f_{v,i-1}=f_{v,0}$ is required: $f_{v,0}$ may represent a measure of the defects in the paste before the loading process. If this information is already contained in the constant elasticity $\mathbf{C}^{(pp)}$ of the pure paste then $f_{v,0}$ can be assumed equal to zero. The concrete two-phase composite has mortar as matrix and gravel as inclusions; at the *i*th iteration, the average stress $\overline{\boldsymbol{\sigma}}^{(m)}$ in the mortar of the concrete two-phase composite subject to $\boldsymbol{\sigma}^{\infty}$ is given by

$$\overline{\boldsymbol{\sigma}}^{(m)}=\mathbf{B}^{(m)}\left(f_{v,i-1}\right)\boldsymbol{\sigma}^{\infty} \tag{3}$$

where $\mathbf{B}^{(m)}\left(f_{v,i-1}\right)$ is the average stress concentration tensor of the mortar in the concrete and depends on $\overline{\mathbf{D}}^{(c)}\left(f_{v,i-1}\right)$ and $\overline{\mathbf{D}}^{(m)}\left(f_{v,i-1}\right)$, as well as on the constant compliance $\mathbf{D}^{(g)}$ of the gravel. Then, the average stress $\overline{\boldsymbol{\sigma}}^{(m)}$ evaluated in (3) becomes the far-field stress applied on the mortar two-phase composite, which has paste as matrix and sand as inclusions; at the *i*th iteration, the average stress $\overline{\boldsymbol{\sigma}}^{(p)}$ in the paste of the mortar two-phase composite subject to $\overline{\boldsymbol{\sigma}}^{(m)}$ is

$$\overline{\boldsymbol{\sigma}}^{(p)}=\mathbf{B}^{(p)}\left(f_{v,i-1}\right)\overline{\boldsymbol{\sigma}}^{(m)} \tag{4}$$

where $\mathbf{B}^{(p)}\left(f_{v,i-1}\right)$ is the average stress concentration tensor of the paste in the mortar and depends on $\overline{\mathbf{D}}^{(m)}\left(f_{v,i-1}\right)$ and $\overline{\mathbf{D}}^{(p)}\left(f_{v,i-1}\right)$, as well as on the constant compliance $\mathbf{D}^{(s)}$ of the sand. Finally, the average stress $\overline{\boldsymbol{\sigma}}^{(p)}$ evaluated in (4) becomes the far-field stress applied on the paste two-phase composite, which has pure paste as matrix and voids as inclusions. The average stress $\overline{\boldsymbol{\sigma}}^{(pp)}$ in the pure paste of the paste two-phase composite subject to $\overline{\boldsymbol{\sigma}}^{(p)}$ is evaluated by using the stress average theorem:

$$\overline{\boldsymbol{\sigma}}^{(pp)}=\overline{\boldsymbol{\sigma}}^{(p)}\Big/\left(1-f_{v,i-1}\right) \tag{5}$$

Once $\overline{\boldsymbol{\sigma}}^{(pp)}$ has been evaluated at the *i*th iteration by means of (5), it is possible to determine the corresponding average strain $\overline{\boldsymbol{\varepsilon}}^{(pp)}$ in the pure paste:

$$\overline{\boldsymbol{\varepsilon}}^{(pp)}=\mathbf{D}^{(pp)}\overline{\boldsymbol{\sigma}}^{(pp)} \tag{6}$$

where $\mathbf{D}^{(pp)}$ is the constant compliance of the pure paste. The value of the void volume fraction at the current *i*th iteration is given by

$$f_{v,i}=f_{v,0}+f_{v,m}\left|\overline{\varepsilon}_{m}^{(pp)}\right|^{\alpha}+f_{v,eq}\overline{\varepsilon}_{eq}^{(pp)\beta} \tag{7}$$

where

$$\overline{\varepsilon}_{m}^{(pp)}=\frac{\overline{\varepsilon}_{11}^{(pp)}+\overline{\varepsilon}_{22}^{(pp)}+\overline{\varepsilon}_{33}^{(pp)}}{3},\quad \overline{e}_{ij}^{(pp)}=\overline{\varepsilon}_{ij}^{(pp)}-\overline{\varepsilon}_{m}^{(pp)}\delta_{ij},\quad \overline{\varepsilon}_{eq}^{(pp)}=\sqrt{\frac{2}{3}\overline{e}_{ij}^{(pp)}\overline{e}_{ij}^{(pp)}} \tag{8}$$

and $\overline{\varepsilon}_{ij}^{(pp)}$ are the components of the second-order strain tensor $\overline{\boldsymbol{\varepsilon}}^{(pp)}$ in (6), equal to the symmetric part of the displacement gradient. Relation (7) is the evolution law of the voids in the paste and depends on the following five parameters: $f_{v,0}$, $f_{v,m}$, $f_{v,eq}$, α, β. If the error $\left|f_{v,i}-f_{v,i-1}\right|$ is less than or equal to a given tolerance then further iterations are not necessary and the average stress and strain evaluated in the current *i*th iteration are correct; otherwise, the void volume fraction $f_{v,i}$ in the current *i*th iteration provided by (7) becomes the value of f_v to consider at the

beginning of the successive iteration $i+1$. In the iteration $i+1$, the relations (2)-(7) are evaluated again by substituting $f_{v,i}$ for $f_{v,i-1}$ into (2)-(5). The average stress $\boldsymbol{\sigma}^{\infty}$ prescribed to the concrete composite represents the input load and must be less than or equal to the strength of the concrete which is unknown. If the prescribed stress $\boldsymbol{\sigma}^{\infty}$ is greater than concrete strength then $f_{v,i}$ at an iteration i usually results greater than one, causing the stopping of the iterative procedure as a void volume fraction f_v greater than one is physically unacceptable. Moreover, the void volume fraction $f_{v,i}$ at the generic ith iteration should not be excessively large as the used homogenization methods provide acceptable estimates if the volume fraction of the inclusions is not so large.

Damage and failure of brittle and ductile materials are very sensitive to the Von Mises equivalent stress and strain, which are often encountered in damage and failure criteria of materials, as well as in the proposed evolution law (7) in the form of $\overline{\varepsilon}_{eq}^{(pp)}$ defined in (8). The parameter $f_{v,eq}$ is used to weight the influence of the Von Mises equivalent strain $\overline{\varepsilon}_{eq}^{(pp)}$ on the void evolution. On the other hand, the parameter $f_{v,m}$ has been introduced in the evolution law (7) in order to take into account also a void growth in presence of hydrostatic compression characterized by $\overline{\varepsilon}_{11}^{(pp)} = \overline{\varepsilon}_{22}^{(pp)} = \overline{\varepsilon}_{33}^{(pp)} < 0$ and $\overline{\varepsilon}_{eq}^{(pp)} = 0$: in this case, no void evolution could occur if $f_{v,m}$ was equal to zero.

In the proposed model, the damage is smeared over the whole volume of concrete while in the post-peak behavior the damage localizes in limited zones [18]. For this reason the proposed model, valid in the pre-peak range, results not suitable to capture the post-peak behavior. In this work, the pre-peak behavior provides essential information, such as the initial Young's modulus of concrete and the compressive strength in multi-axial stress state.

In the load case of prescribed uni-axial compression, the uni-axial stress can be plotted against the uni-axial strain so as to obtain the compressive stress-strain curve of concrete. The stress-strain curves provided in [17] in the load case of uni-axial compression exhibit a maximum compressive stress denoted by σ_p, which represents the compressive strength σ_c of concrete. In [17], the proposed micromechanical model has been used in order to capture peculiar aspects of the stress-strain curve in the load case of uni-axial compression:

- in most concrete materials, a higher compressive strength is associated with a higher initial tangent Young's modulus E_0;
- the formation and evolution of voids in the cement paste cause a reduction of the tangent line to the stress-strain curve;
- a higher w/c ratio of water to cement involves a concrete with a lower compressive strength σ_c and a lower tangent line E_0 at the origin of the stress-strain curve;
- the concrete materials having the same initial stiffness E_0 also have the same σ_p/ε_p ratio of peak stress to peak strain, as predicted by phenomenological curves [19]; ε_p is the strain corresponding to σ_p in the concrete stress-strain curve.

In this work, the micromechanical model presented in [17] and briefly described in this paragraph is used in order to predict the failure surface of cement concrete subject to multi-axial compression. Firstly, further analyses with uni-axial compression are presented in the next paragraph.

INFLUENCE OF THE MODEL PARAMETERS ON THE UNI-AXIAL COMPRESSIVE STRESS-STRAIN CURVE

The iterative procedure previously described is used to estimate the stress-strain curve $\sigma_{11} - \varepsilon_{11}$ of concrete subject to uni-axial compression: in this stress state, concrete is subject to the average stress $\overline{\boldsymbol{\sigma}}^{(c)}$ and all the components of $\overline{\boldsymbol{\sigma}}^{(c)}$ are equal to zero except $\overline{\sigma}_{11}^{(c)} = \sigma_{11}^{\infty} < 0$. In Fig. 1, the normal stress $\sigma_{11} = -\overline{\sigma}_{11}^{(c)}$ is plotted against the normal strain $\varepsilon_{11} = -\overline{\varepsilon}_{11}^{(c)}$ of concrete subject to uni-axial compression, where $\overline{\boldsymbol{\varepsilon}}^{(c)}$ is the average strain in concrete.

In the examples of this work, the constituents pure paste, sand and gravel are considered homogeneous, isotropic and linear elastic; they have the geometrical and mechanical properties reported in Tab. 1. The parameters of the evolution law (7) adopted for the curves of Fig. 1 assume the following values. In the solid black curves of Fig. 1, $f_{v,eq}$ varies between 30 and 50, β is equal to 0.7, α, $f_{v,0}$ and $f_{v,m}$ are assumed equal to zero. In the solid red curves of Fig. 1, $f_{v,eq}$ varies

between 30 and 50, β is equal to 0.8, α, $f_{v,0}$ and $f_{v,m}$ are assumed equal to zero. In the green curves of Fig. 1, $f_{v,0}$ is assumed equal to zero, $f_{v,m}$ varies between 10 and 20, $f_{v,eq}$ is equal to 30, α and β are assumed equal to 0.8.

The tangent line to a curve of Fig. 1 at the origin of the ε_{11} - and σ_{11} -axes is the overall initial stiffness E_0. Each curve of Fig. 1 has a maximum denoted by σ_p and attained when $\varepsilon_{11} = \varepsilon_p$. The tangent line to the curves of Fig. 1 at the end-point $(\varepsilon_p, \sigma_p)$ is about horizontal. In case of uni-axial compression, the peak σ_p of the stress-strain curve represents the compressive strength σ_c of concrete.

The curves of Fig. 1 have the same initial stiffness E_0: in fact, E_0 depends on the properties reported in Tab. 1 and the initial porosity $f_{v,0}$, which are constants that do not vary among the curves of Fig. 1. The curves with a given value of β have the same ratio σ_p/ε_p: e.g. in the black curves characterized by $\beta = 0.7$, the ratio σ_p/ε_p is about $E_0/2$; in the red and green curves characterized by $\beta = 0.8$, the ratio σ_p/ε_p is always constant and is greater than $E_0/2$. The exponent $\beta = 0.7$ was chosen in order to have $\sigma_p = E_0\varepsilon_p/2$, as predicted by the following phenomenological curve proposed by Desayi and Krishnan [19]

$$\sigma_{11}(\varepsilon_{11}) = \frac{E_0\varepsilon_{11}}{1+\left(\varepsilon_{11}/\varepsilon_p\right)^2} \tag{9}$$

The generic curve of Fig. 1 is obtained by connecting the point $(\varepsilon_{11}, \sigma_{11})$; the end-point of this curve is $(\varepsilon_p, \sigma_p)$, whose coordinates are used to have the dimensionless curve $(\varepsilon_{11}/\varepsilon_p, \sigma_{11}/\sigma_p)$. In Fig. 2, σ_{11}/σ_p is plotted against $\varepsilon_{11}/\varepsilon_p$ for the eight curves of Fig. 1. The eight dimensionless curves of Fig. 2 are the same; this behavior is also exhibited by the experimental stress-strain curves and the curve (9).

Constituent	Young's modulus	Poisson's ratio	Volume fractions in cement concrete
Gravel	45 GPa	0.23	0.4
Sand	65 GPa	0.21	0.326
Cement paste	-	-	0.274
Pure paste	15 GPa	0.22	-

Table 1: Geometrical and mechanical properties of the four-phase composite.

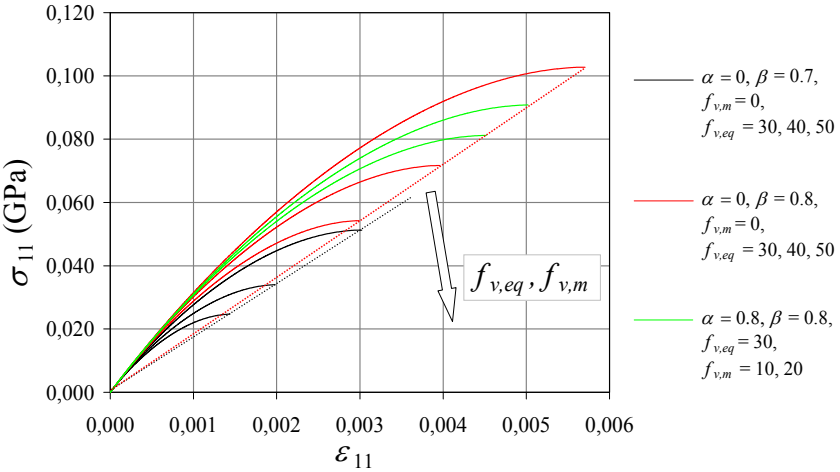

Figure 1: Stress-strain curves of concrete in uni-axial compression.

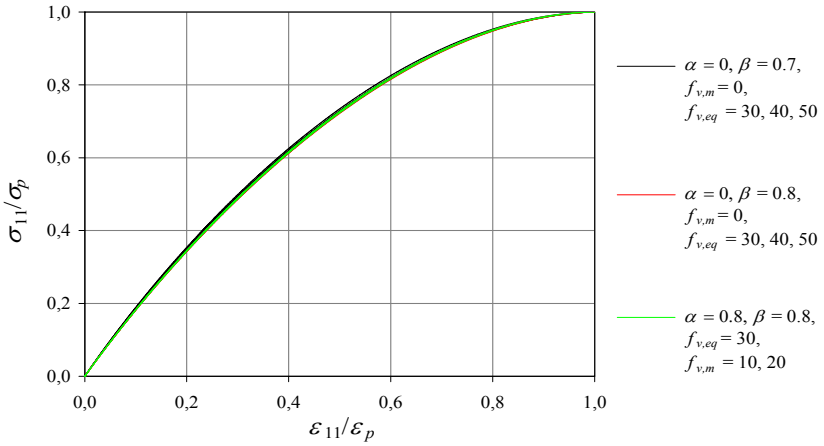

Figure 2: Dimensionless stress-strain curves of concrete in uni-axial compression.

COMPRESSIVE FAILURE SURFACES

The proposed model can also be used to determine the behavior of cement concrete in load cases of multi-axial compression. This is done in this work, where the failure surface of concrete subject to bi-axial or tri-axial compression is determined by using the previously described iterative procedure. The objective is to represent the compressive failure surface of cement concrete in the space of the eigenvalues of the average stress $\overline{\boldsymbol{\sigma}}^{(c)}$ in concrete. The eigenvalues are the principal stresses in concrete and are contained in the vector $\boldsymbol{\sigma}_c = \left[\sigma_{c1}\ \sigma_{c2}\ \sigma_{c3}\right]^{\mathrm{T}}$. The generic direction in the space of the eigenvalues of $\overline{\boldsymbol{\sigma}}^{(c)}$ is represented by the unit vector $\mathbf{n}_\sigma = \left[\hat{\sigma}_1\ \hat{\sigma}_2\ \hat{\sigma}_3\right]^{\mathrm{T}}$. The proposed method determines the average strain $\overline{\boldsymbol{\varepsilon}}^{(c)}$ in cement concrete subject to a prescribed stress $\boldsymbol{\sigma}_c = \left[\gamma\hat{\sigma}_1\ \gamma\hat{\sigma}_2\ \sigma_{c3}\ \right]^{\mathrm{T}}$, where γ is a positive parameter which increases during the loading process; $\hat{\sigma}_1$, $\hat{\sigma}_2$ and σ_{c3} are constants with $\hat{\sigma}_1 \le 0$ and $\hat{\sigma}_2 \le 0$. The principal directions of $\overline{\boldsymbol{\sigma}}^{(c)}$ coincide with the coordinate axes, i.e. $\boldsymbol{\sigma}_c = \left[\gamma\hat{\sigma}_1\ \gamma\hat{\sigma}_2\ \sigma_{c3}\ \right]^{\mathrm{T}} = \left[\sigma_{11}^{(c)}\ \sigma_{22}^{(c)}\ \sigma_{33}^{(c)}\ \right]^{\mathrm{T}}$. In order to determine a point of the failure surface, the loading parameter γ increases from zero up to the admissible maximum value $\gamma_{\max}$. The above-mentioned iterative procedure is executed for each value of γ. After the admissible values of γ have been determined for given directions $\hat{\sigma}_1$ and $\hat{\sigma}_2$ and given stress σ_{c3}, the stress $\sigma_{ii} = -\sigma_{ii}^{(c)}$ for $i = 1,\ 2$ can be plotted against the corresponding strain $\varepsilon_{ii} = \left|\overline{\varepsilon}_{ii}^{(c)}\right|$ so as to obtain a $\sigma_{ii} - \varepsilon_{ii}$ stress-strain curve in the ith direction. From a physical point of view, it is interesting to consider the $\sigma_{ii} - \varepsilon_{ii}$ stress-strain curve when $\hat{\sigma}_j \ge \hat{\sigma}_i$ with $i \ne j$, i.e. $\sigma_{ii} \ge \sigma_{jj}$; this curve exhibits a maximum stress denoted by $\left|\sigma_{ii,p}^{(c)}\right|$ and the tangent line to the curve at the maximum is about horizontal. The searched point of the failure surface of cement concrete in multi-axial compression is therefore given by

$$\boldsymbol{\sigma}_c = \boldsymbol{\sigma}_{c,p} = \left[\gamma_{\max}\hat{\sigma}_1\ \ \gamma_{\max}\hat{\sigma}_2\ \ \sigma_{c3}\ \right]^{\mathrm{T}} = \left[\sigma_{11,p}^{(c)}\ \sigma_{22,p}^{(c)}\ \sigma_{c3}\ \right]^{\mathrm{T}} \tag{10}$$

Next, the points $\boldsymbol{\sigma}_{c,p}$ are estimated with the previously described iterative procedure and assuming $\mathbf{n}_\sigma = \left[\hat{\sigma}_1\ \hat{\sigma}_2\ 0\right]^{\mathrm{T}}$ with $\hat{\sigma}_1 < 0$ and $\hat{\sigma}_2 < 0$, i.e. a bi-axial compression is imposed to cement concrete. In this case, the points $\boldsymbol{\sigma}_{c,p}$ represent a failure curve in the negative quadrant of the plane with σ_{c1}- and σ_{c2}-axes. In Fig. 3, the failure curves are illustrated for the cement concrete characterized by the geometric and mechanical properties reported in Tab. 1. The parameters of the evolution law (7) adopted for the curves of Fig. 3 have the same values assumed in Fig. 1: e.g., in the solid black curves of Fig. 3, $f_{v,0} = f_{v,m} = \alpha = 0$, $f_{v,eq} = 30,\ 40,\ 50$, $\beta = 0.7$. The failure curves exhibit an elliptical shape and the curves

characterized by $f_{v,m}=0$ have values of $\gamma_{\max}$ greater than the uni-axial compressive strength σ_c. The failure curves reflect the uni-axial behavior observed in Fig. 1: for a given direction $\mathbf{n}_\sigma=\left[\hat{\sigma}_1\ \hat{\sigma}_2\ 0\right]^{\mathrm{T}}$, $\gamma_{\max}$ decreases with increasing $f_{v,eq}$ and $f_{v,m}$.

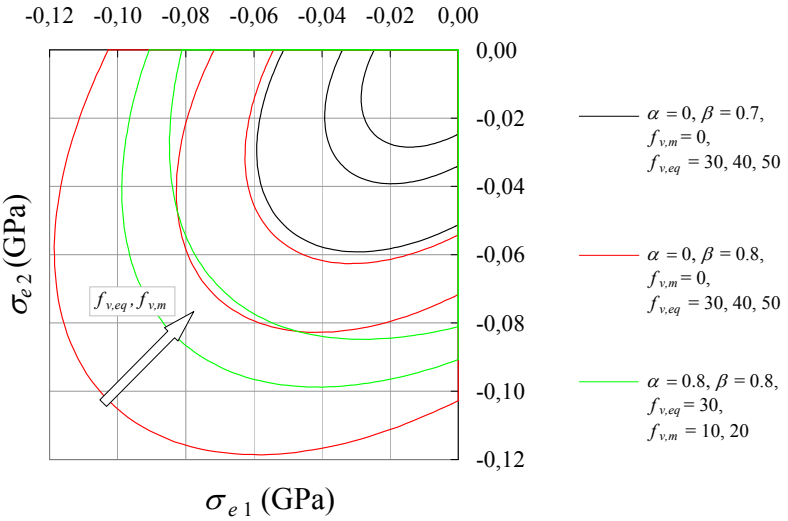

Figure 3: Failure curves in bi-axial compression.

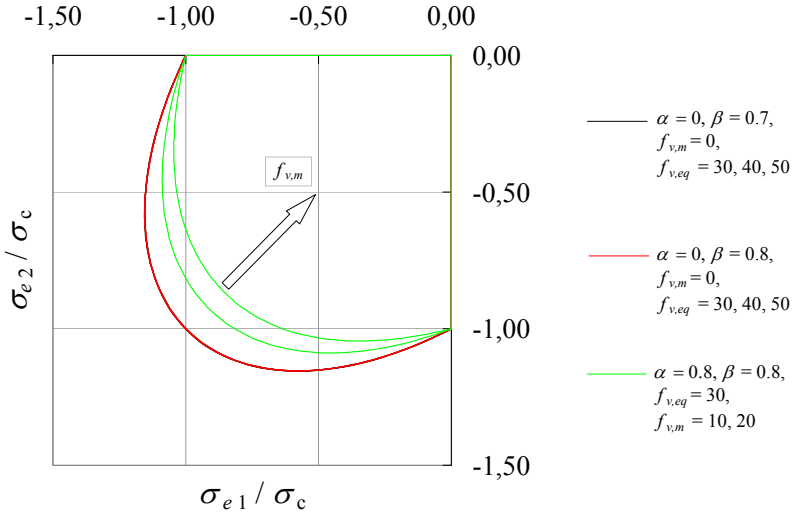

Figure 4: Dimensionless failure curves in bi-axial compression.

The generic curve of Fig. 3 is obtained by connecting the points $(\sigma_{e1},\sigma_{e2},0)=\gamma_{\max}(\hat{\sigma}_1,\ \hat{\sigma}_2,0)$; this curve intersects the coordinate axes at the points $(-\sigma_c,0,0)$ and $(0,-\sigma_c,0)$, where σ_c is the uni-axial compressive strength of concrete and is used to determine the dimensionless curve $(\hat{\sigma}_1,\ \hat{\sigma}_2,0)\gamma_{\max}/\sigma_c$. In Fig. 4, the eight curves of Figure 3 are plotted in the dimensionless form: these curves depend on the parameter $f_{v,m}$. In fact, the curves characterized by $f_{v,m}=0$ are the same whatever the parameter β is, whereas the remaining curves vary with $f_{v,m}$: the area bounded by the dimensionless failure curve decreases with increasing $f_{v,m}$. Fig. 4 shows that the adopted values of $f_{v,m}$ should be small as large values of $f_{v,m}$ provide a bi-axial compressive strength $\gamma_{\max}\sqrt{2}/2$ less than the uni-axial compressive strength when the average stress $-\gamma\left(\sqrt{2}/2,\sqrt{2}/2,0\right)$ is prescribed on concrete, in contrast with the experimental failure curve of concrete.

In Fig. 5, six failure curves are plotted: the black curves refer to $f_{v,m}=0$ whereas the turquoise curves refer to $f_{v,m}=10$. Moreover, the solid curves are the failure curves in bi-axial compression; the dotted curves are the intersection of the failure surfaces with the plane $\sigma_{e3}=0.01$ GPa, where σ_{e3} is the third of the three coordinate axes of the stress space where the failure surface is plotted; the dashed curves are the intersection of the failure surfaces with the plane $\sigma_{e3}=-0.01$ GPa (for the dotted and dashed curves, the load direction is different from $\mathbf{n}_\sigma=\left[\hat{\sigma}_1\ \hat{\sigma}_2\ 0\right]^T$). As it is expected, the admissible domain bounded by the failure curve increases in presence of a negative σ_{e3} (compression) and decreases in presence of a positive σ_{e3} (traction).

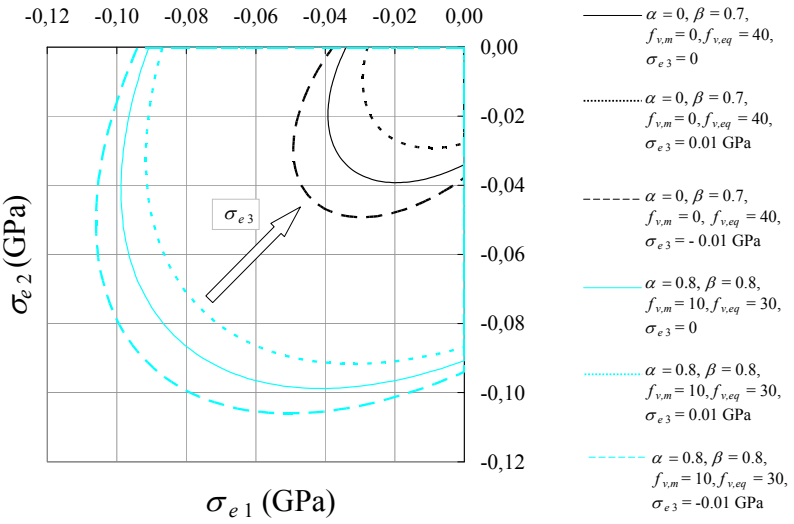

Figure 5: Failure curves in bi-axial and tri-axial compression.

Conclusions

In this work, a micromechanical model is used for estimating the failure curves of cement concrete in bi-axial and tri-axial compression. The concrete failure is due to the creation and evolution of voids in the cement paste. The void evolution decreases the tangent stiffness to the concrete stress-strain curve and the concrete compressive strength is attained when this tangent line becomes horizontal. This condition is used to determine the failure curves of concrete in bi-axial and tri-axial compression. Mori-Tanaka and Eshelby homogenization methods are used to determine the overall behavior of concrete. The micromechanical analyses show which values of the void evolution parameters represent better the concrete behavior. As a future development, micromechanical methods different from the Mori-Tanaka one will be used and different evolution laws of the voids will be considered in the attempt to capture better the multi-axial concrete behavior.

Acknowledgments

This research was carried out in the framework of the DPC/ReLUIS 2014 – AQ DPC/ReLUIS 2014-2016 project (theme: reinforced concrete structures) funded by the Italian Department of Civil Protection.

References

[1] Bruno, D., Greco, F., Lonetti, P., Blasi, P.N., Sgambitterra, G., An investigation on microscopic and macroscopic stability phenomena of composite solids with periodic microstructure, International Journal of Solids and Structures, 47 (2010) 2806-24.

[2] Caporale, A., Luciano, R., Micromechanical analysis of periodic composites by prescribing the average stress, Annals of Solid and Structural Mechanics, 1 (2010) 117-137.
[3] Greco, F., Leonetti, L., Lonetti, P., A two-scale failure analysis of composite materials in presence of fiber/matrix crack initiation and propagation, Composite Structures, 95 (2013) 582-97.
[4] Lau, K.-t., Zhou, L.-m., Mechanical performance of composite-strengthened concrete structures, Composites Part B: Engineering, 32 (2001) 21-31.
[5] Aprile, A., Benedetti, A., Coupled flexural-shear design of R/C beams strengthened with FRP, Composites Part B: Engineering, 35 (2004) 1-25.
[6] Agbossou, A., Michel, L., Lagache, M., Hamelin, P., Strengthening slabs using externally-bonded strip composites: Analysis of concrete covers on the strengthening, Composites Part B: Engineering, 39 (2008) 1125-35.
[7] D'Ambrisi, A., Feo, L., Focacci, F., Bond-slip relations for PBO-FRCM materials externally bonded to concrete, Composites Part B: Engineering, 43 (2012) 2938-49.
[8] D'Ambrisi, A., Feo, L., Focacci, F., Experimental analysis on bond between PBO-FRCM strengthening materials and concrete, Composites Part B: Engineering, 44 (2013) 524-32.
[9] Milani, G., Esquivel, Y.W., Lourenço, P.B., Riveiro, B., Oliveira, D.V., Characterization of the response of quasi-periodic masonry: Geometrical investigation, homogenization and application to the Guimarães castle, Portugal, Engineering Structures, 56 (2013) 621-41.
[10] Caporale, A., Parisi, F., Asprone, D., Luciano, R., Prota, A., Micromechanical analysis of adobe masonry as two-component composite: Influence of bond and loading schemes, Composite Structures, 112 (2014) 254-63.
[11] Yang, C.C., Huang, R., A two-phase model for predicting the compressive strength of concrete, Cement and Concrete Research, 26 (1996) 1567-77.
[12] Yang, C.C., Approximate elastic moduli of lightweight aggregate, Cement and Concrete Research, 27 (1997) 1021-30.
[13] Yang, C.-C., Huang, R., Approximate strength of lightweight aggregate using micromechanics method, Advanced Cement Based Materials, 7 (1998) 133-8.
[14] Li, G., Zhao, Y., Pang, S.-S., Four-phase sphere modeling of effective bulk modulus of concrete, Cement and Concrete Research, 29 (1999) 839-45.
[15] Hashin, Z., Monteiro, P.J.M., An inverse method to determine the elastic properties of the interphase between the aggregate and the cement paste, Cement and Concrete Research, 32 (2002) 1291-300.
[16] Hernández, M.G., Anaya, J.J., Ullate, L.G., Ibañez, A., Formulation of a new micromechanic model of three phases for ultrasonic characterization of cement-based materials, Cement and Concrete Research, 36 (2006) 609-16.
[17] Caporale, A., Feo, L., Luciano, R., Damage mechanics of cement concrete modeled as a four-phase composite, Composites Part B: Engineering, In Press. http://dx.doi.org/10.1016/j.compositesb.2014.02.006
[18] Watanabe, K., Niwa, J., Yokota, H., Iwanami, M., Experimental study on stress-strain curve of concrete considering localized failure in compression, Journal of Advanced Concrete Technology, 2 (2004) 395-407.
[19] Desayi, P., Krishnan, S., Equation for the stress–strain curve of concrete, ACI J 61 (1964) 345–50.